ACS APPLIED ELECTRONIC MATERIALS

pubs.acs.org/acsaelm

Article

Hybrid Intelligence-Driven Nanopolymeric Sensor for Precise Electrochemical Vitamin C Analysis, Free from LoD: Application in Real Lemon Juice

Emre Dokuzparmak,* Emine Sezer, Timuçin Güner, Esra Yaşar, Hilal Özçelik, and Sinan Akgöl

Cite This: ACS Appl. Electron. Mater. 2025, 7, 6980−6993

Read Online

ACCESS | Metrics & More | Article Recommendations

ABSTRACT: This study presents the design, synthesis, and systematic evaluation of an electrochemical nanosensor platform tailored for the precise and selective quantification of vitamin C. The sensor architecture integrates His-functionalized poly(2-hydroxyethyl methacrylate-*co*-ethylene glycol dimethacrylate) (His-pHEG) polymeric nanoparticles onto Nafion-modified screen-printed carbon electrodes (SPCE), thereby providing a bioactive interface with enhanced analyte affinity and stability. The His-pHEG nanoparticles were synthesized via emulsion polymerization and covalently grafted with L-histidine, as confirmed by FTIR, SEM, and zeta potential analyses. This functionalization endowed the nanoparticles with enhanced affinity and high selectivity toward vitamin C molecules, while ensuring colloidal stability and uniform morphology. Sensor fabrication parameters, including Nafion film thickness and polymer concentration, were systematically optimized to maximize electrochemical performance. The resulting His-pHEG/Nafion-modified SPCE demonstrated superior analytical characteristics, achieving a low limit of detection and a broad linear dynamic range, as determined by cyclic voltammetry and differential pulse voltammetry measurements. To overcome the fundamental limitations of conventional calibration-based electrochemical methods, such as nonlinearity and variability, a two-stage hybrid machine learning framework, specifically tailored to the inherent nature of the sensor data, was developed and integrated into the sensing workflow. The two-stage model utilized CatBoost classification to distinguish analyte presence, followed by CatBoost regression to estimate vitamin C concentration, with hyperparameter optimization ensuring robustness and predictive accuracy. Real-sample validation using lemon juice confirmed the sensor's high recovery rates and practical applicability, demonstrating reliable performance in complex matrices. This multidisciplinary approach bridges polymer chemistry, nanotechnology, electrochemical sensing, and artificial intelligence to deliver a portable, cost-effective, and highly sensitive vitamin C detection system. Future efforts will focus on translating this platform into mobile-based, real-time analytical devices, enabling on-site applications in food quality control, healthcare, and pharmaceutical industries.

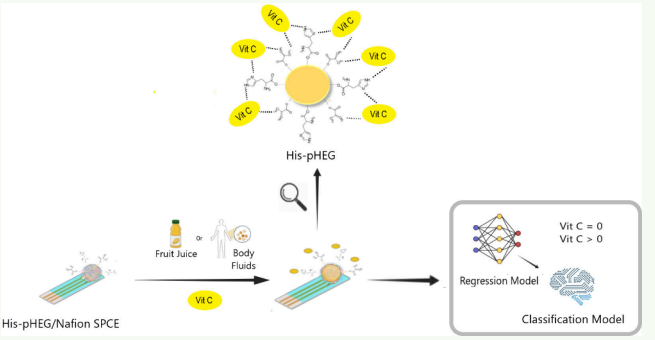

KEYWORDS: *polymeric nanoparticle, grafting, vitamin C, nanosensor, machine learning, hybrid model, artificial intelligence*

1. INTRODUCTION

Ascorbic acid (Vitamin C, AA), a water-soluble compound, is an essential micronutrient for human physiology, primarily due to its potent antioxidant properties and its critical enzymatic roles in collagen biosynthesis, iron absorption, and immune modulation.[1−3] A fundamental physiological constraint is the human body's inability to synthesize or store Vitamin C, necessitating consistent dietary intake.[4,5] Deficiency of this nutrient can cause scurvy, impaired immunity, and delayed wound healing, whereas excessive intake may lead to oxidative stress and iron metabolism imbalance.[6−12] Given these health implications, accurate quantification of Vitamin C is essential, especially in citrus-based products, where its levels fluctuate due to storage, processing, and environmental factors.

Under current food safety regulations and increasing consumer demand for accurate nutritional labeling, Vitamin C plays a role beyond its nutritional function. It is widely used for its antioxidant properties, pH regulation, and contribution to product stability.[5,13,14] Maintaining optimal Vitamin C levels supports both nutritional quality and alignment with interna-

Received: April 25, 2025
Revised: June 30, 2025
Accepted: July 11, 2025
Published: July 18, 2025

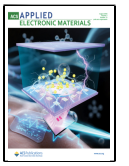

tional food safety and health standards.[15−19] Despite its importance, conventional food analysis methods face limitations such as matrix interference, lengthy procedures, and the high cost of advanced instrumentation.[20] Therefore, advanced sensing technologies are needed for fast, cost-effective, and accurate Vitamin C detection, especially in complex foods like citrus-based drinks.

Various analytical methods have been used to quantify Vitamin C, each with its own strengths and weaknesses.[21−25] Titration is simple and inexpensive but lacks specificity and is affected by oxidation interference.[26] Paper spray mass spectrometry offers high sensitivity and minimal sample preparation but is costly, affected by ion suppression, and requires expert data analysis.[27] Spectrophotometric methods are fast but vulnerable to matrix interference, reducing reliability.[28] High-performance liquid chromatography provides high sensitivity and specificity but is expensive and needs skilled operators, limiting routine use.[24−29]

Electrochemical sensors have become a promising alternative, providing high sensitivity, low detection limits, and real-time, on-site analysis.[29,30] Screen-printed electrodes (SPCE) are especially advantageous due to their low cost, scalability, and portability.[31,32] However, traditional electrochemical sensors face challenges such as nonlinearity, signal drift, and environmental effects, requiring improvements through nanomaterials and polymer surface modifications.[33−35]

Nanomaterials and surface-grafted polymers are pivotal in enhancing the sensitivity and selectivity of electrochemical sensors. Surface-grafted polymeric films introduce well-defined binding sites, improving analyte recognition and minimizing nonspecific interactions, thus enhancing measurement accuracy in complex matrices.[36,37] These modifications significantly improve electron transfer efficiency and sensor stability, rendering them particularly advantageous for field-deployable biosensors.[38] Among polymer-based systems, grafted polymer architectures are especially promising for Vitamin C detection due to their ability to fine-tune molecular interactions, ensuring higher selectivity and reproducibility.[39−41] Surface grafting techniques enable the precise functionalization of sensor interfaces, optimizing their affinity for ascorbic acid and extending their applicability beyond food analysis to biomedical and environmental monitoring.[42−46] These properties position grafted polymeric materials as a transformative approach for next-generation electrochemical sensing platforms.[47,48]

Electrochemical sensors offer real-time, portable detection but face accuracy issues from nonlinearity, environmental changes, and signal saturation. Traditional calibration methods cannot handle these challenges, so machine learning is increasingly applied to enhance sensor accuracy.[49,50,75]

Machine learning (ML) approaches in electrochemical analysis include classification and regression models, each providing key benefits. Classification assigns data to discrete categories and improves detection of low-concentration analytes, reducing false positives and negatives through algorithms like Logistic Regression, Random Forest, XGBoost, CatBoost, and Artificial Neural Networks (ANN).[51−57] Regression models, including Linear Regression, Support Vector Regression, Random Forest Regressor, XGBoost Regressor, and CatBoost Regressor, enable accurate quantification by capturing nonlinear sensor responses that traditional calibration curves often miss.[58,59] Together, these ML methods enhance the reliability and precision of electrochemical sensing.

Hybrid ML models combine multiple algorithms to capitalize on their strengths, improving predictive accuracy across applications.[60−62] A two-stage hybrid framework integrates classification and regression to enhance electrochemical sensing, classification first detects the presence of the analyte, ensuring regression-based concentration estimates are applied only to positive samples. This prevents errors from zero-concentration samples and mitigates signal saturation effects, boosting accuracy in real-time analysis.

This study proposes a novel hybrid ML approach for Vitamin C detection that combines classification to distinguish detectable from nondetectable samples with regression to accurately quantify concentration. Unlike traditional calibration methods, this framework employs adaptive learning to dynamically adjust sensor performance under varying conditions. The novelty of this research lies not only in the synergistic integration of nanopolymeric sensor technology with AI-driven electrochemical modeling, but more importantly, in how this integration is executed. Specifically, our work departs from standard ML applications by developing a unique hybrid workflow that combines classification and regression stages to target the inherent challenges of electrochemical sensors, including nonlinearity, signal saturation, and noise. This integrated approach ultimately establishes a more robust and reliable analytical methodology that liberates the sensor's performance from the constraints of traditional calibration methods, even in complex matrices. By combining polymer grafting with hybrid ML intelligence, the platform aims to deliver precise, real-time, on-site Vitamin C analysis while overcoming limitations of conventional electrochemical sensors.

This work presents the fabrication and optimization of a His-pHEG/Nafion-modified SPCE for the electrochemical detection of Vitamin C in lemon juice. By synthesizing histidine-functionalized poly(2-hydroxyethyl methacrylate) (His-pHEG) nanoparticles and optimizing key electrochemical parameters, the sensor achieves enhanced selectivity, sensitivity, and stability. A hybrid machine learning model combining classification and regression improves analyte detection and quantification, addressing limitations of traditional calibration methods such as signal nonlinearity and drift. This integrated approach combines established electrochemical techniques with machine learning-based adaptive sensing, improving analytical performance and demonstrating strong potential for applications in food safety, nutrition monitoring, and biomedical fields. To our knowledge, this is the first study to combine His-pHEG nanoparticles, Nafion/SPCE architecture, and a two-stage hybrid ML framework for Vitamin C analysis, demonstrating high accuracy and real-sample applicability in complex matrices.

2. MATERIALS AND METHODS

This section delineates the materials, synthesis procedures, characterization techniques, sensor fabrication strategy, electrochemical analysis protocols, and machine learning integration employed in this study. The experimental workflow encompasses the synthesis and functionalization of His-pHEG polymeric nanoparticles, their structural and morphological characterization, the construction of the modified SPCE sensor, and the application of voltametric techniques for vitamin C detection. Additionally, the integration of a hybrid machine learning model is detailed to demonstrate its role in

https://doi.org/10.1021/acsaelm.5c00822
ACS Appl. Electron. Mater. 2025, 7, 6980−6993

enhancing analytical performance and overcoming conventional electrochemical limitations.

2.1. Chemicals and Apparatus. L-Ascorbic acid, 2-hydroxyethyl methacrylate (HEMA), ethylene glycol dimethacrylate (EGDMA), and L-histidine (His) were obtained from Sigma-Aldrich (USA). Other chemicals, including tetrahydrofuran (THF), sodium hydride (NaH), vaseline parafilm, ethanol (C_2H_5OH), nitrogen gas (N_2), potassium persulfate (KPS), and poly(vinyl alcohol) (PVA), were of analytical grade and used without further purification. Centrifugation processes were carried out using Centurion Scientific benchtop centrifuges (UK). All electrochemical measurements were performed using a PalmSens BV portable potentiostat (The Netherlands).

2.2. Synthesis and Functionalization of His-pHEG Polymeric Nanoparticles. The fabrication of poly(2-hydroxyethyl methacrylate)-*co*-ethylene glycol dimethacrylate (pHEG) polymeric nanoparticles was accomplished via a surfactant-free emulsion polymerization protocol. Initially, 0.6 mL of HEMA and 0.3 mL of EGDMA monomers were introduced into a polymerization vessel containing 0.5 g poly(vinyl alcohol) (PVA) dissolved in 50 mL of distilled water, serving as a stabilizing agent. The resulting mixture was subjected to ultrasonic agitation for 10 min to ensure homogeneity. Subsequently, an initiator solution comprising 39.6 mg potassium persulfate (KPS) in 90 mL of distilled water was incorporated. The polymerization medium was further degassed with nitrogen gas for 5 min to eliminate dissolved oxygen, and the reaction was conducted at 70 °C under continuous stirring at 100 rpm for 5 h. The synthesized nanoparticles were harvested via centrifugation at 10,000 rpm, followed by sequential washing with an ethanol:water (1:1, v/v) mixture and drying at 50 °C.

Surface functionalization of the pHEG nanoparticles was performed through covalent grafting with L-histidine to augment their binding affinity toward ascorbic acid. Specifically, 2 g of dried pHEG nanoparticles were dispersed in ethanol and pretreated by centrifugation to achieve a stable precipitate. A catalyst solution consisting of 181 mg sodium hydride (NaH) and 300 mg L-histidine dissolved in 10 mL tetrahydrofuran (THF) was then introduced into the reaction medium. The grafting reaction proceeded at 45 °C for 24 h under continuous agitation. Upon completion, the modified nanoparticles were collected via centrifugation at 3000 g and subjected to thorough washing with ethanol and distilled water to remove residual reagents. The synthetic strategy and molecular modifications are schematically illustrated in Figure 1.

2.3. Characterization of His-pHEG Polymeric Nanoparticles. The chemical structure and surface morphology of the synthesized His-pHEG polymeric nanoparticles were characterized using FTIR spectroscopy, scanning electron microscopy (SEM), and zeta potential analysis. FTIR spectra were recorded with an FTIR 8000 Series spectrometer (Shimadzu, Japan) to confirm polymerization and successful grafting of L-histidine. SEM analysis (Philips XL-30S FEG) was employed to observe nanoparticle morphology and size distribution, following gold–palladium coating of the dried samples. Zeta potential and particle size measurements were performed using dynamic light scattering (DLS), where 1 mL of nanoparticle suspension was analyzed to evaluate surface charge and colloidal stability.

2.4. Fabrication of the His-pHEG/SPCE Sensor. The fabricated His-pHEG polymeric nanoparticles were immobilized onto the working electrode surface via a Nafion matrix to ensure uniform dispersion and film stability. Specifically, a 0.5% Nafion solution was prepared to suspend the polymeric nanoparticles, and 15 μL of this suspension was drop-cast onto the surface of the SPCE. The electrode was subsequently dried in an oven at 37 °C for 60 min to achieve stable film formation (Figure 2). Following drying, the modified electrodes were stored at 4 °C under controlled conditions until further electrochemical analysis.

2.5. Electrochemical Detection of Vitamin C Using the His-pHEG/SPCE Sensor. Electrochemical measurements were conducted using a portable potentiostat to evaluate the performance of the fabricated nanobiosensor. DPV and CV techniques were employed to characterize the electrochemical behavior of the His-pHEG/Nafion-modified SPCE. For the redox probe, a 5 mM solution of ferricyanide/ferrocyanide ($[Fe(CN)_6]^{3-/4-}$) in 0.1 M phosphate-buffered saline (PBS) was prepared, exploiting the reversible redox reactions of iron species.

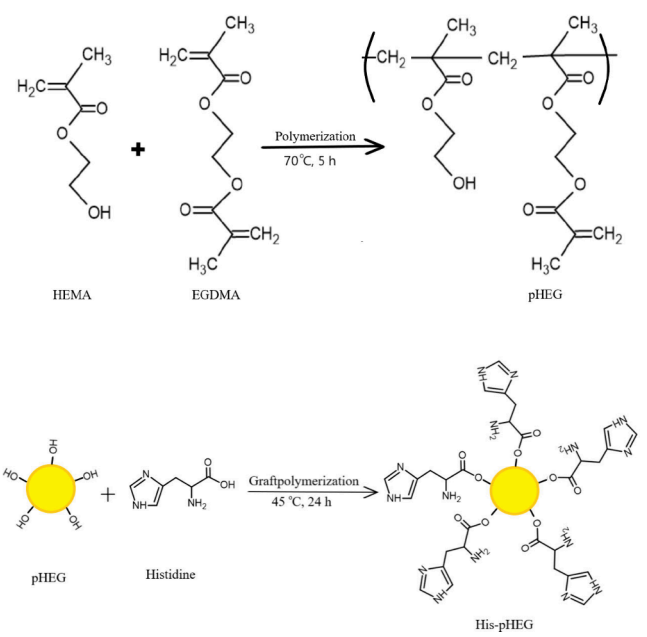

Figure 1. Schematic representation of the molecular structure of the pHEG polymeric nanoparticle and an illustration of the grafting reaction.

The presence of the His-pHEG polymeric nanoparticle layer on the electrode surface acts as a bioactive barrier, impeding electron transfer by limiting the accessibility of the redox probe to the conductive electrode interface. This results in a measurable decrease in peak current, which is proportional to the amount of nanoparticles immobilized on the surface. Calibration curves were constructed based on the DPV response, and the limit of detection (LoD) and limit of quantification (LoQ) were calculated using the standard deviation method, as LoD = 3.3 × SD and LoQ = 10 × SD.[63] DPV measurements were performed within a potential window of − 0.20 V to +0.60 V, using a scan rate of 60 mV/s. The electrochemical characterization and subsequent optimization steps ensured the stability and sensitivity of the sensor system.

2.6. Machine Learning-Assisted Hybrid Modeling for Electrochemical Vitamin C Quantification. To address the inherent challenges associated with conventional calibration-based electrochemical approaches, particularly sensor nonlinearity, environmental variability, signal drift, and detection constraints defined by LoD and LoQ, a hybrid ML framework was designed and implemented. This hybrid framework integrates classification and regression models within a two-stage architecture, enhancing the overall accuracy, reliability, and adaptability of electrochemical vitamin C quantification as illustrated in Figure 3.

In the first stage of the hybrid model, classification algorithms were employed to categorize samples based on the presence or absence of vitamin C. This preliminary step plays a critical role in preventing the propagation of erroneous predictions, particularly in low-concentration or nondetectable samples, which are prone to signal noise and misclassification in traditional systems. A comprehensive suite of classification algorithms, including Logistic Regression, Random Forest, XGBoost, CatBoost, and ANN, was systematically evaluated. Model performance was assessed through standard evaluation metrics, namely precision, recall, accuracy, and F1-score, providing a multidimensional assessment of classification efficacy. To mitigate the inherent imbalance observed in the data set, particularly between analyte-positive and analyte-negative samples, a stratified data set balancing strategy was employed, ensuring equitable representation

https://doi.org/10.1021/acsaelm.5c00822
ACS Appl. Electron. Mater. 2025, 7, 6980−6993

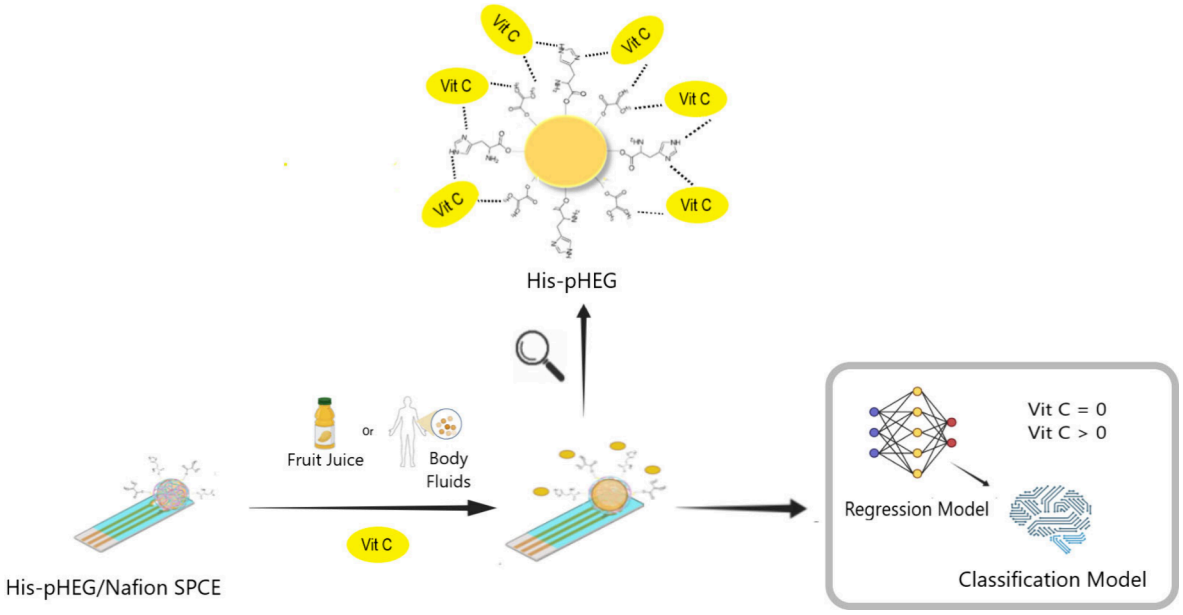

Figure 2. Illustration of the fabrication process and detection mechanism of vitamin C.

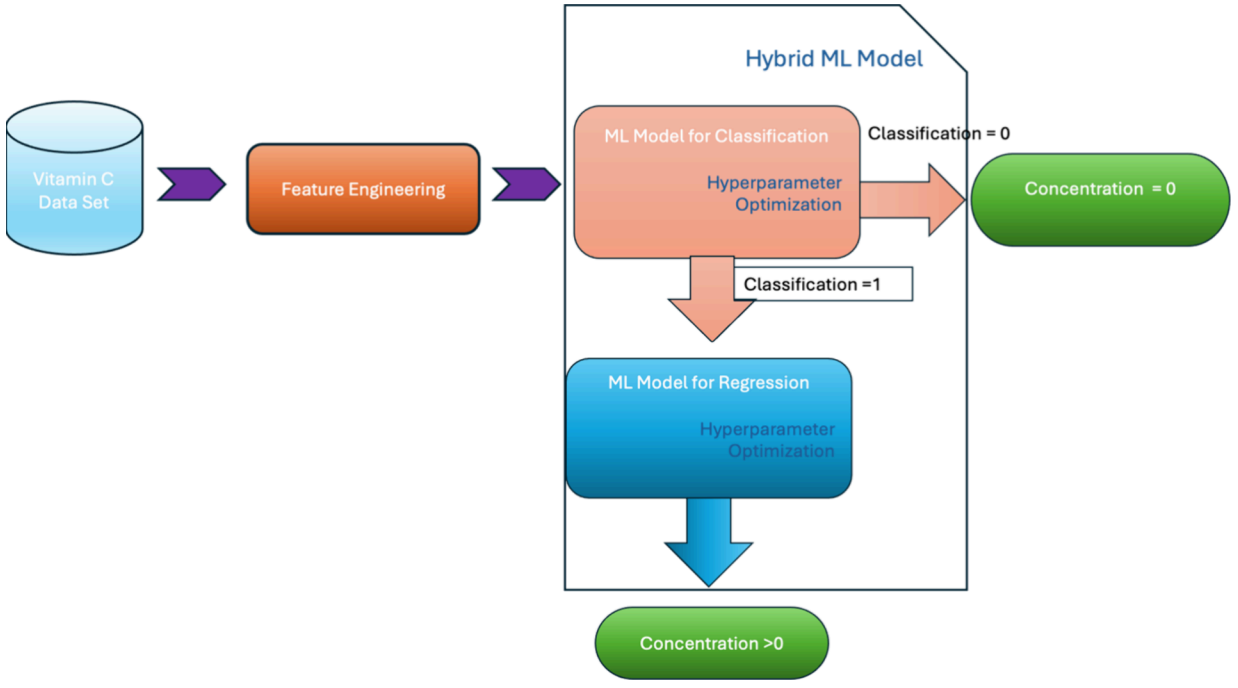

Figure 3. Components of the hybrid ML model.

across the concentration spectrum and preserving model generalizability.

Furthermore, to maximize classification performance and enhance model robustness, a thorough hyperparameter optimization process was implemented. Both Bayesian search and grid search techniques were utilized to systematically explore and fine-tune critical model parameters, such as tree depth, learning rate, number of estimators, and regularization factors. Special emphasis was placed on addressing the class imbalance issue through explicit adjustment of the class_weight parameter. By assigning a higher weight to the vitamin C-negative class, the model's sensitivity and specificity were significantly improved, reducing the risk of false-positive predictions and enhancing detection fidelity at low analyte concentrations.

Upon successful classification, the regression phase was initiated to accurately quantify vitamin C concentrations in analyte-positive samples. A range of advanced regression algorithms, including XGBRegressor, LightGBM Regressor, CatBoost Regressor, Random Forest Regressor, and SVR, was deployed to model the nonlinear relationship between electrochemical response signals and analyte concentration levels. Regression model performance was evaluated using established metrics, including Mean Absolute Error (MAE), Root Mean Squared Error (RMSE), coefficient of determination (R^2 Score), Explained Variance Score, and Cross-Validation R^2 Score, providing a robust statistical foundation for model comparison and selection.

In parallel to the classification stage, hyperparameter optimization for the regression models was rigorously performed utilizing Bayesian optimization and grid search methodologies. Parameters such as learning rate, maximum tree depth, regularization terms (L1 and L2 penalties), number of iterations, and minimum child weight were

https://doi.org/10.1021/acsaelm.5c00822
ACS Appl. Electron. Mater. 2025, 7, 6980−6993

iteratively tuned to minimize prediction error, enhance model stability, and improve generalization across varying concentration ranges. This comprehensive optimization strategy ensured that the regression models were not only tailored to the specific electrochemical data set but also resilient to fluctuations in experimental conditions and sensor variability.

To integrate and holistically evaluate both classification and regression stages, a composite evaluation metric, designated as the Hybrid Score, was introduced. The Hybrid Score amalgamates classification accuracy, regression precision, and model stability metrics into a unified framework, enabling systematic ranking and selection of the optimal model configuration. This hybrid intelligence approach, grounded in advanced machine learning techniques, allows the sensor system to dynamically adapt to real-time experimental conditions, effectively circumventing the limitations of conventional electrochemical methods and delivering reliable, precise vitamin C quantification across a broad analytical range. This two-stage architecture represents more than a simple application of ML; it establishes a novel methodological framework for sensor data analysis by logically sequencing the analyte detection (classification) and quantification (regression) steps. Consequently, a unique composite metric was also employed to holistically evaluate the framework's overall efficacy.

3. RESULTS AND DISCUSSION

The results of the present study are presented and discussed in the following sections, encompassing the physicochemical characterization of the synthesized His-pHEG polymeric nanoparticles, the evaluation of the modified electrochemical behavior, and the performance assessment of the hybrid machine learning model. The systematic approach integrates material characterization techniques with electrochemical and computational analyses, providing a comprehensive understanding of sensor performance. The key findings elucidate the efficacy of surface modifications, nanoparticle functionalization, and machine learning-assisted hybrid modeling in enhancing the accuracy, sensitivity, and applicability of the developed sensor system.

3.1. Synthesis and Characterization of His-pHEG Polymeric Nanoparticles. The physicochemical characterization of the synthesized His-pHEG polymeric nanoparticles was conducted to verify the structural integrity, morphological uniformity, and colloidal stability of the developed system. Three analytical techniques, FTIR spectroscopy, scanning electron microscopy (SEM), and zeta potential measurements, were employed to comprehensively evaluate the nanoparticle properties following polymerization and surface functionalization.

3.1.1. Fourier Transform Infrared Spectroscopy (FTIR) Analysis. FTIR spectroscopy was employed to confirm the chemical structure of the synthesized His-pHEG nanoparticles and to verify the successful grafting of L-histidine onto the polymer matrix. The comparative FTIR spectra of pHEG and His-pHEG nanoparticles are presented in Figure 4, clearly illustrating the structural differences following the functionalization process. Broad bands observed at 3481 cm^{-1} and 3413 cm^{-1} were assigned to O−H stretching vibrations, indicative of hydroxyl groups present in the polymer backbone.[69−71] A band at 2948 cm^{-1} was attributed to C−H stretching vibrations. The strong absorption band appearing at 1726 cm^{-1} corresponded to the ester carbonyl (C═O) stretching vibration, confirming successful polymerization of HEMA.[69]

Furthermore, the presence of the amide functional groups introduced by histidine grafting was evidenced by the moderate-intensity bands at 1454 cm^{-1} and 1393 cm^{-1}, corresponding to C−O and N−H (amide) vibrations, respectively. Additionally, characteristic bands associated with the imidazole ring of histidine, including C═C, C−N, and N−H bonds, were clearly observed, providing conclusive evidence of successful surface functionalization. All obtained results are in strong concordance with the findings reported in the existing literature.[69−71] These spectral findings confirm the incorporation of L-histidine into the polymeric structure, validating the efficiency of the grafting process.

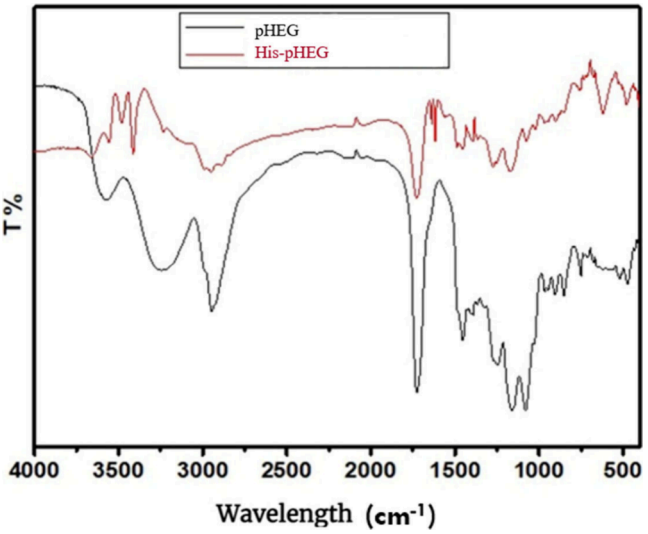

Figure 4. Comparative FTIR spectra of pHEG and His-pHEG polymeric nanoparticles.

3.1.2. Scanning Electron Microscope (SEM) Analysis. SEM analysis was performed to elucidate the morphological characteristics and size distribution of the synthesized polymeric nanoparticles. Representative SEM micrographs of both pHEG and His-pHEG nanoparticles are presented in Figure 5, highlighting the morphological differences arising from the histidine grafting process. As observed, both nanoparticle types exhibited a uniform, spherical morphology with smooth surface textures and a narrow particle size distribution, consistent with the polydispersity index (PDI) results obtained during synthesis. Notably, no evidence of significant aggregation or structural deformation was detected following the surface modification, indicating that the functionalization process preserved the structural integrity of the polymeric matrix. Furthermore, the homogeneous distribution and monodispersity observed in Figure 5 confirm the efficiency of the synthesis and functionalization protocols, thereby ensuring the suitability of the nanoparticles for subsequent sensor fabrication.

3.1.3. Zeta Size Analysis. Dynamic light scattering (DLS) and zeta potential analyses were employed to evaluate the size distribution and surface charge properties of both grafted and ungrafted polymeric nanoparticles. The results demonstrated that the synthesized nanoparticles exhibited a narrow particle size distribution, as evidenced by a low polydispersity index (PDI) value of 0.042. This low PDI value indicates high uniformity and monodispersity, corroborating the morphological observations obtained from SEM analysis.

The average hydrodynamic diameter of the polymeric nanoparticles was determined to be approximately 348 nm for both pHEG and His-pHEG samples, in agreement with the particle dimensions observed in SEM micrographs. Zeta

https://doi.org/10.1021/acsaelm.5c00822
ACS Appl. Electron. Mater. 2025, 7, 6980−6993

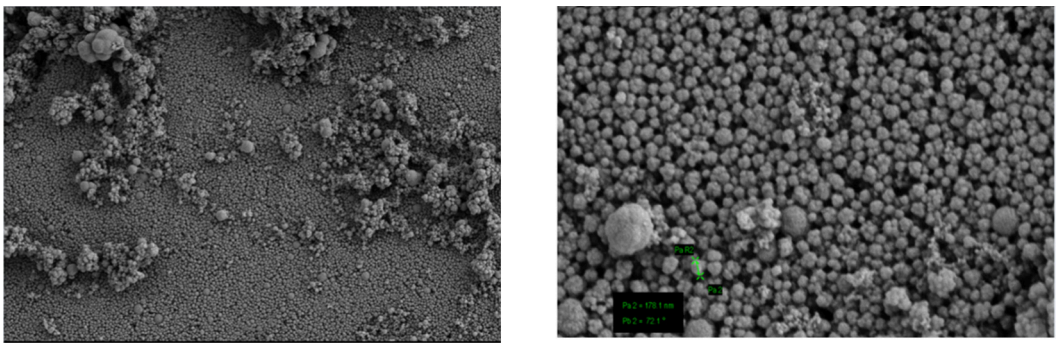

Figure 5. SEM micrographs of pHEG polymeric nanoparticles (left) and His-pHEG polymeric nanoparticles (right).

potential measurements further revealed that the His-pHEG nanoparticles possessed a negative surface charge, with a measured potential of − 4.6 mV, as depicted in Figure 6. This

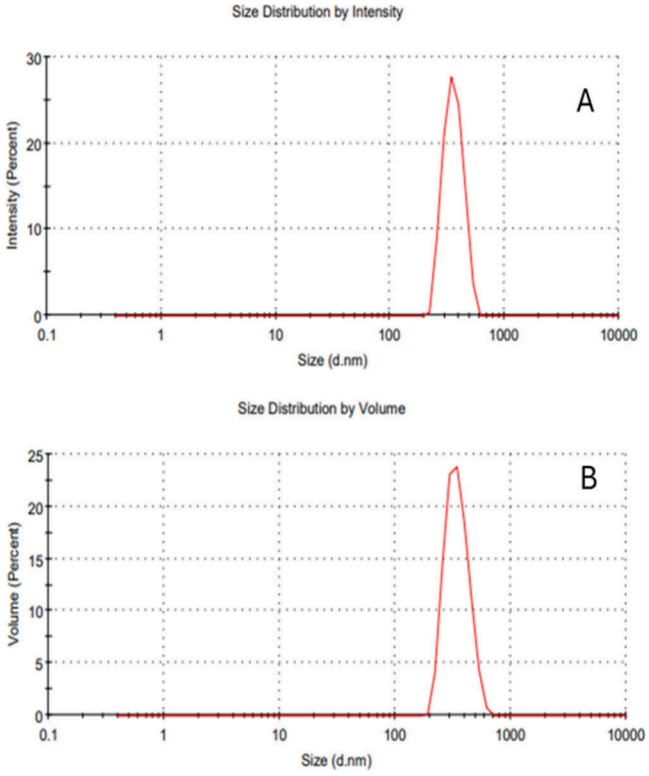

Figure 6. Zeta size analysis of (A) pHEG polymeric nanoparticles and (B) His-pHEG polymeric nanoparticles.

negative zeta potential can be attributed to the presence of ionizable functional groups, including carboxyl and imidazole moieties introduced via histidine grafting, which contribute to the electrostatic stability of the nanoparticle suspension by preventing aggregation. The combination of narrow size distribution and stable surface charge confirms the suitability of the synthesized nanoparticles for subsequent electrochemical sensor applications.

3.2. Fabrication Steps of His-pHEG/Nafion-SPCE. The electrochemical performance of the His-pHEG/Nafion-modified SPCE sensor was systematically assessed to elucidate the effect of surface modifications on electron transfer characteristics. Cyclic voltammetry (CV) measurements were employed after each modification step to monitor changes in current response and evaluate the contribution of each layer to the overall sensor behavior.

As illustrated in Figure 7, the bare SPCE electrode exhibited a baseline redox response when measured in 5 mM

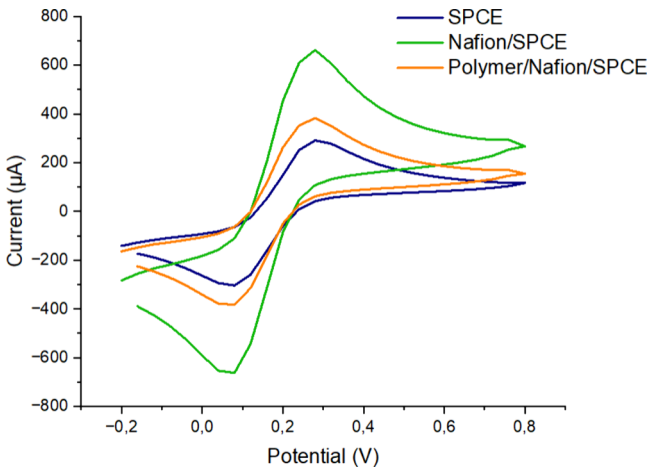

Figure 7. CVs of SPCE, Nafion/SPCE, and His-pHEG/Nafion-SPCE in 5 mM $[Fe(CN)_6]^{3-/4-}$ in 0.1 M PBS.

$[Fe(CN)_6]^{3-/4-}$ solution containing 0.1 M PBS. Following the deposition of a 0.5% Nafion film, a significant increase in current response was observed, attributed to the high ionic conductivity and favorable film-forming properties of the Nafion polymer. However, subsequent immobilization of 0.8 mg/mL His-pHEG polymeric nanoparticles onto the Nafion/SPCE surface resulted in a notable decrease in current. This reduction is attributed to the nonconductive nature of the grafted polymeric layer, which introduces an electrochemical barrier and hinders the diffusion of redox species to the electrode surface.

3.2.1. Influence of Nafion Film Thickness in Electrochemical Sensing. To optimize sensor performance, the effect of Nafion film thickness on peak current response was systematically investigated. Nafion solutions containing 0.5% polymer and 0.6 mg/mL His-pHEG were applied to the SPCE surface in varying volumes of 5, 10, 15, and 20 μL. As depicted in Figure 8, the peak current increased proportionally with Nafion volume up to 15 μL, indicating enhanced conductivity and improved electron transfer. However, further increasing the volume to 20 μL resulted in a decline in current response, likely due to the formation of an excessively thick film that restricts the diffusion of $[Fe(CN)_6]^{3-/4-}$ ions, thereby impeding reaction kinetics. Consequently, a Nafion film

https://doi.org/10.1021/acsaelm.5c00822
ACS Appl. Electron. Mater. 2025, 7, 6980−6993

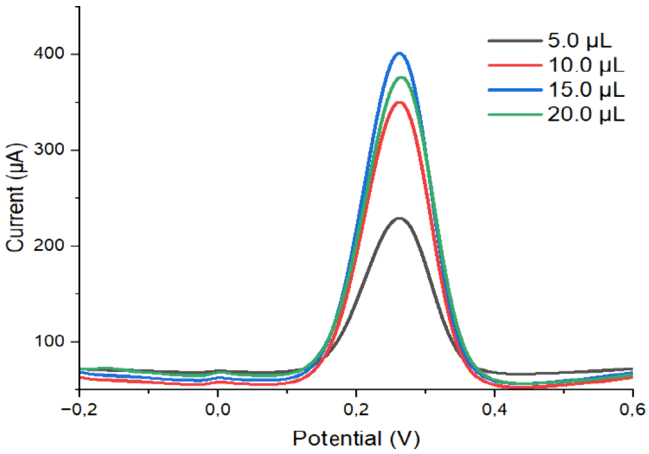

Figure 8. Effect of varying volumes of His-pHEG/Nafion, ranging from 5 to 20 μL, on the DPV measurements was evaluated in a 5 mM $[Fe(CN)_6]^{3-/4-}$ solution within 0.1 M PBS.

volume of 15 μL was determined as optimal for maximizing electrochemical performance.

3.2.2. Effect of Polymer Concentration. The concentration of the His-pHEG polymer also plays a critical role in modulating the sensor's electrochemical behavior due to its inherently low conductivity. To identify the optimal concentration, varying amounts of His-pHEG, ranging from 0 to 1 mg/mL, were immobilized onto the SPCE surface in combination with the previously optimized Nafion film. As shown in Figure 9, the current response initially increased with

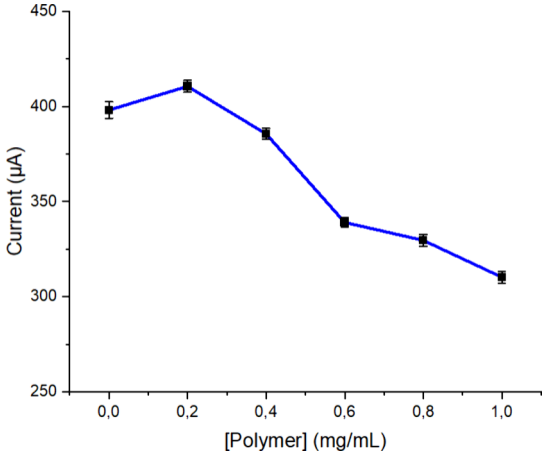

Figure 9. DPV peak values of the His-pHEG/Nafion-modified SPCE were measured in $[Fe(CN)_6]^{3-/4-}$ within 0.1 M PBS, using different concentrations of His-pHEG ranging from 0 to 1 mg/mL.

increasing polymer concentration, reaching a maximum at 0.8 mg/mL. Concentrations beyond this value resulted in decreased current, likely due to the formation of a denser polymeric layer that limits electron transfer by creating an insulating barrier. Therefore, 0.8 mg/mL His-pHEG was selected as the optimal concentration, ensuring a balance between adequate surface coverage and maximal electrochemical signal output.

3.3. Analytical Performance of His-pHEG/Nafion-Modified SPCE. The analytical performance of the His-pHEG/Nafion-modified SPCE sensor was systematically evaluated for the detection of vitamin C. Differential pulse voltammetry (DPV) measurements were conducted using a series of vitamin C concentrations (0.05, 0.1, 0.15, 0.25, 0.3, and 0.5 mg/mL) applied onto the polymeric nanoparticle-coated electrode under previously optimized conditions. These measurements were conducted to evaluate the sensor's sensitivity, linearity, and limit of detection.

As illustrated in Figure 10, the DPV responses exhibited a well-defined increase in peak current with rising vitamin C concentrations, indicating efficient interaction between the analyte and the sensor surface. The calibration curve demonstrated excellent linearity within the concentration range of 0.28 to 11.36 μM, yielding a correlation coefficient (R^2) of 0.9962. LoD and LoQ were calculated as 0.09 μM and 0.73 μM, respectively, under optimal electrochemical conditions (5.0 mM $[Fe(CN_6)]^{3-/4-}$ in 0.1 M PBS).

Comparative evaluation with similar sensor systems reported in the literature highlights the superior sensitivity of the developed His-pHEG/Nafion-modified SPCE sensor. Notably, the achieved LoD value of 0.09 μM is significantly lower than those reported in many previous studies,[64−68] underscoring the enhanced detection capabilities of the proposed platform. A detailed comparison of the analytical performance parameters between this study and previously reported vitamin C sensors is summarized in Table 1. Additionally, the wide linear dynamic range supports its applicability for accurate quantification across diverse vitamin C concentrations.

The enhanced analytical performance is primarily attributed to the synergistic effects of the surface modifications. The grafting of L-histidine onto the pHEG polymeric nanoparticles provided a high-affinity interface for vitamin C binding, while the Nafion layer contributed to surface stability and facilitated efficient electron transfer. Collectively, these modifications resulted in improved sensitivity, stability, and reproducibility.

These findings demonstrate that the developed sensor represents a rapid, cost-effective, and portable alternative to conventional vitamin C detection methods, offering substantial potential for real-world applications in food quality control, pharmaceutical analysis, and clinical diagnostics.

3.4. Determination of Vitamin C in Lemon Juice. To evaluate the applicability of the developed His-pHEG/Nafion-modified SPCE sensor for real sample analysis, vitamin C quantification was performed on lemon juice samples. Fresh lemon juice was diluted with 0.1 M phosphate-buffered saline (PBS) to prepare three different concentration levels. The prepared samples were subsequently applied onto the polymer-coated electrode surface, followed by a drying period of 60 min under optimal conditions established in prior sensor studies.

DPV measurements were conducted under the optimized electrochemical conditions in Figure 11. The current responses obtained from the lemon juice samples demonstrated a clear, concentration-dependent increase, which closely correlated with the established vitamin C calibration curve. This observation confirmed the sensor's ability to detect vitamin C within complex sample matrices.

Lemon juice samples were diluted at different Lemon Juice (mL)/Total Solution (mL) ratios, specifically 5/20, 10/20, and 20/20. DPV measurements were performed using these diluted samples, and the current responses of the sensor system were recorded. Analysis of the obtained current values (Figure 11) revealed that the calculated concentration values were 0.0567 ± 0.001, 0.1102 ± 0.001, and 0.1472 ± 0.001, respectively (Table 2). These results indicate a strong

https://doi.org/10.1021/acsaelm.5c00822
ACS Appl. Electron. Mater. 2025, 7, 6980−6993

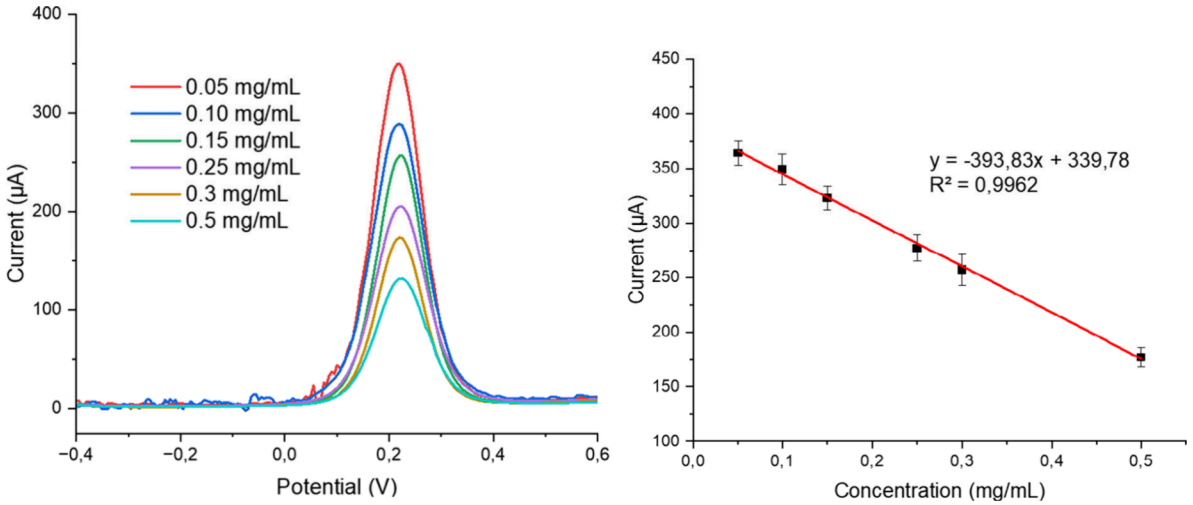

Figure 10. DPV analysis of varying concentrations of vitamin C in 5.0 mM $[Fe(CN_6)]^{3-/4-}$ in 0.1 M PBS.

Table 1. Comparison of This Study with Previously Reported Vitamin C Sensors

Electrode	Method	LoD	Linear range	ref.
AA-Polymer/Nafion/SPE	DPV	0.09 μM	0.28 μM to 11.36 μM	This Study
AA-MIPs/MXene/GCE	DPV-CV	0.27 μM	0.5 μM to 10 μM	48
AA-MIPCH sensor (Colorimetric MIP Sensor)	-	0.011 μM	0.02 μM to 0.10 μM	49
AA-MIP/SPCE	SWV	0.11 μM	0.45−13.52 μM and 13.52− 409.10 μM	50
AA-NCNF	CV	20 μM	50 μM to 1000 μM	51
VitC/PGSE	CV and SWSV	0,4 μM	1,0−400 μM	52

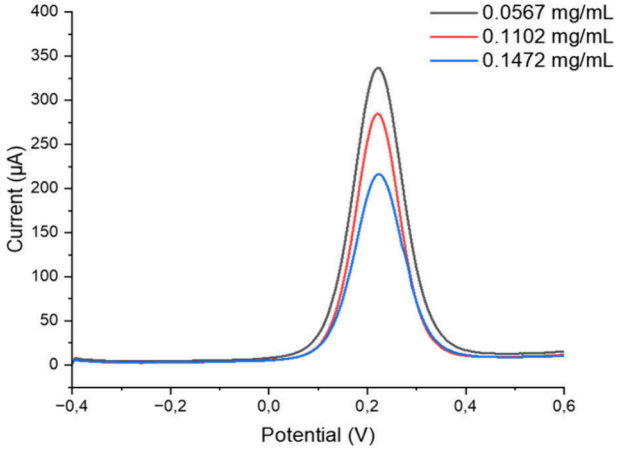

Figure 11. DPV analysis of lemon juice samples under optimal conditions.

correlation between concentration changes and current responses.

Table 2. Percent Recovery Results of Lemon Juice at Different Concentrations

Lemon Juice Sample (Lemon Juice (mL)/Total Solution (mL)	Measured Concentration (mg/mL)	Expected Concentration (mg/mL)	% Recovery
5/20	0.0567 ± 0.001	0.0550	103.1% ± 2.12
10/20	0.1102 ± 0.001	0.1100	100.2% ± 1.64
20/20	0.1472 ± 0.001	0.1500	98.1% ± 2.61

Accuracy and reliability of the developed biosensor were quantitatively evaluated by calculating the recovery percentage (% recovery) for each concentration level, based on eq 1. The recovery values were determined by comparing the experimentally detected vitamin C concentrations to the corresponding known spiked concentrations, as summarized in Table 2. The recovery percentages ranged from 98.1% to 103.1%, demonstrating the high precision and analytical reliability of the His-pHEG/Nafion-modified SPCE sensor system in real sample analysis.

$$\%\ Recovery = \left(\frac{Measured\ Concentration}{Expected\ Concentration}\right) \times 100 \quad (1)$$

These findings confirm the efficacy of the His-pHEG/Nafion-modified SPCE sensor in accurately quantifying vitamin C in real food samples. The consistent performance across varying concentrations underscores its potential applicability in quality control, food analysis, and beverage industry settings for rapid, cost-effective, and reliable vitamin C determination.

3.5. Reusability of the His-pHEG/Nafion-Modified SPCE Sensor. To assess the reusability of the fabricated SPCE-based sensor, repeated DPV analyses were carried out using a lemon juice sample containing a fixed concentration (0.1102 mg/mL) of vitamin C under optimized experimental conditions. As depicted in Figure 12, the sensor retained more than 80% of its initial response current even after 17 consecutive measurements, indicating a high level of operational stability and reusability. Notably, no significant peak shifts were observed across the measurements, suggesting that sensor drift was negligible throughout the repeated cycles. Furthermore, the consistent current responses and low standard deviation values imply minimal material degradation,

https://doi.org/10.1021/acsaelm.5c00822
ACS Appl. Electron. Mater. 2025, 7, 6980−6993

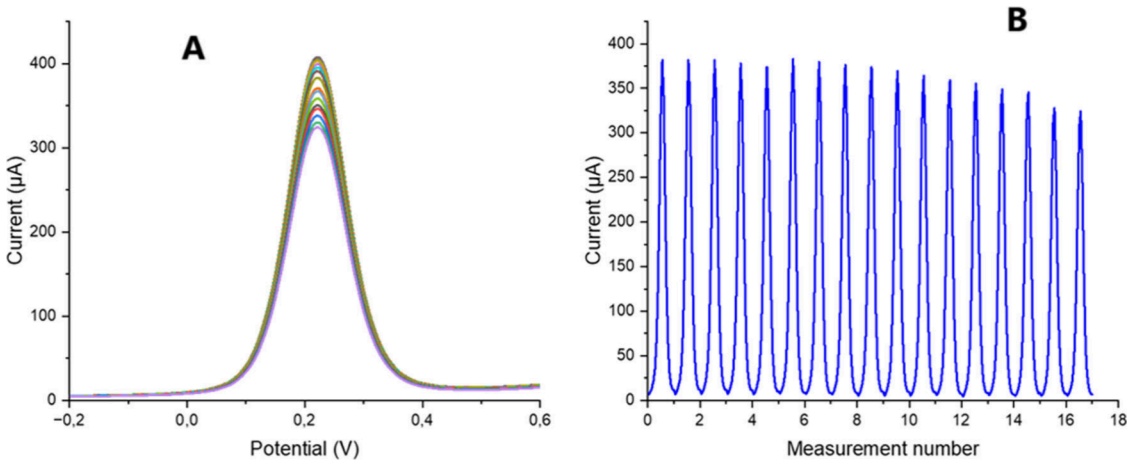

Figure 12. Reusability study of the His-pHEG/Nafion-modified SPCE sensor using DPV under optimized conditions in lemon juice: A) DPV responses obtained, B) Plot of peak current values versus measurement number.

confirming that the sensing layer remained structurally and electrochemically stable. The sustained signal output also suggests that biofouling effects were highly limited in this real sample matrix, underscoring the sensor's robustness in complex environments. Altogether, these findings not only highlight the sensor's potential for practical, real-sample applications but also support its reliability for routine and repeated analyses without significant deterioration in performance.

Recent studies in the literature have demonstrated that electrochemical methods developed for the determination of vitamin C generally exhibit high levels of reusability.[72−74] For instance, in one study, a portable electrochemical sensing system was designed for ascorbic acid detection, and it was reported that approximately 80% of the initial current response was retained after six consecutive measurements.[72] Another study employing a gold-modified SPCE for vitamin C analysis indicated that the sensor preserved around 80% of its original signal after five repeated measurements.[73] Similarly in another current study, electrochemical determination of vitamin C from food samples was performed using graphene platforms modified with gold nanoparticles. It was reported that, after five repeated measurements, the current responses were retained at over 90% of their initial values.[74]

In comparison to these existing approaches, the His-pHEG/Nafion-modified SPCE sensor developed in the present study demonstrated significantly enhanced reusability, as evidenced by the preservation of over 80% of the initial peak current after 17 successive DPV measurements (Figure 12B). Moreover, the anodic peak consistently appeared around +0.2 V throughout the repeated measurements, indicating negligible peak shift and suggesting that sensor drift was effectively absent (Figure 12A). The low standard deviation values obtained across replicates further support the electrochemical stability of the sensor system. Importantly, the maintenance of signal intensity in a complex real sample matrix such as lemon juice implies that the effects of biofouling were minimal. These findings collectively indicate that the sensor operates with high stability and durability, without undergoing significant material degradation under repeated use, thereby reinforcing its potential for reliable application in routine and real-sample analyses.

3.6. Optimization and Performance Evaluation of the Hybrid Machine Learning Model. The hybrid machine learning model developed in this study underwent a rigorous optimization and evaluation process to ensure its accuracy, reliability, and robustness in electrochemical vitamin C detection. Given the inherent challenges in sensor-based electrochemical analysis, such as nonlinear response behaviors, detection variability, and concentration-dependent fluctuations, a structured evaluation approach was implemented to systematically assess classification and regression model performance.

3.6.1. Comparative Analysis and Performance Assessment of Classification Models. To determine the most effective classification model for vitamin C detection, several machine learning algorithms including Logistic Regression, Random Forest, XGBoost, CatBoost, and ANN were trained and tested on the balanced electrochemical data set. The primary objective was to classify whether a given sample contained detectable levels of vitamin C, ensuring that only relevant samples progressed to the regression stage.

The classification models were evaluated based on four key performance metrics: precision, recall, accuracy, F1-score. Due to the initial imbalance in the data set, a stratified resampling technique was employed to ensure equal representation of different vitamin C concentrations, particularly at low concentration levels (including 0 μM). After hyperparameter optimization, CatBoost, a tree-based ensemble method, outperformed traditional algorithms, achieving the highest F1-score and precision values, demonstrating superior capability in correctly identifying vitamin C presence as shown in Table 3. The confusion matrix for each classification model is presented in Figure 13.

To mitigate overfitting, the data set was partitioned into training and test sets, and model performance was assessed on

Table 3. Comparison of Performance Metrics of Classification Models

	Accuracy	Precision	Recall	F-1 Score
Logistic Regression	0.911602	0.831019	0.911602	0.869447
ANN (MLP Classifier)	0.911602	0.831019	0.911602	0.869447
Random Forest	0.848066	0.850183	0.848066	0.849120
XGBoost	0.875691	0.853587	0.875691	0.863810
CatBoost	0.908840	0.870356	0.908840	0.877370

https://doi.org/10.1021/acsaelm.5c00822
ACS Appl. Electron. Mater. 2025, 7, 6980−6993

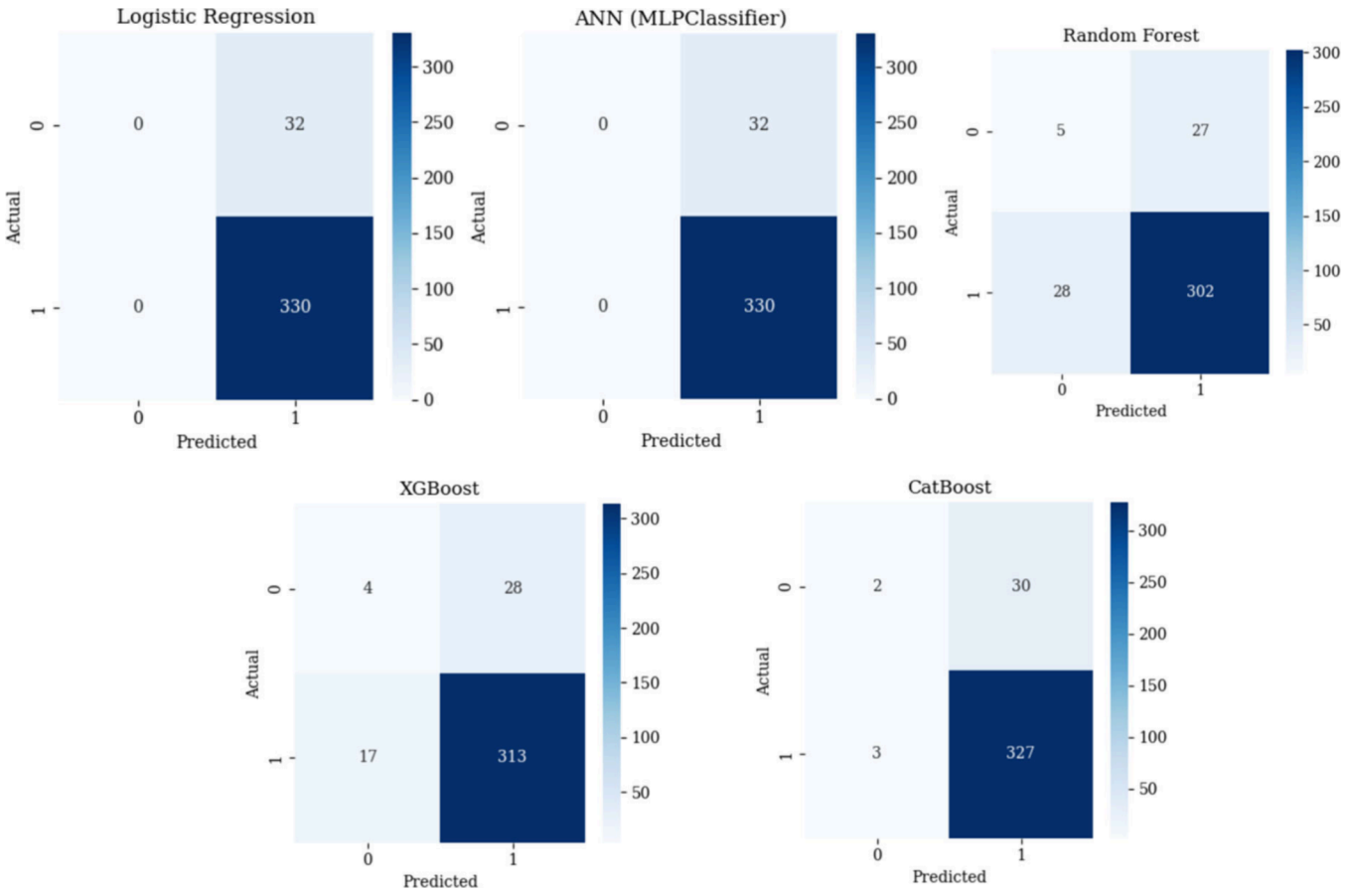

Figure 13. Confusion matrix for classification models.

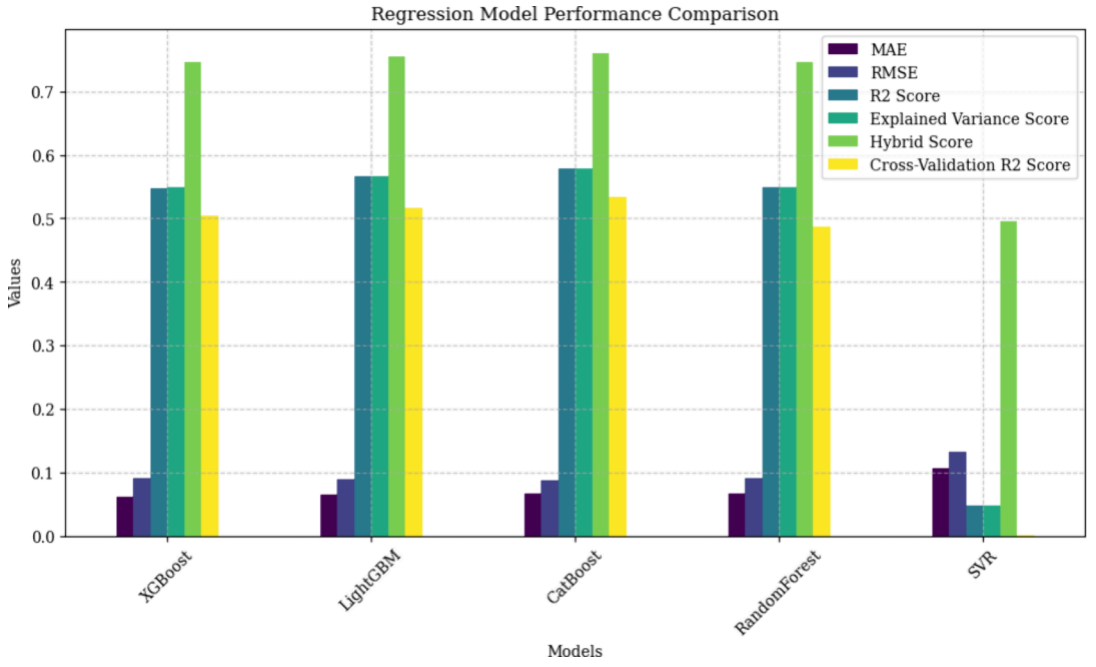

Figure 14. Comparison of regression model performances.

both subsets to evaluate generalization capability. Additionally, cross-validation techniques, including k-fold cross-validation, were employed to ensure model robustness across multiple data partitions. Among the evaluated models, CatBoost demonstrated the highest stability, achieving a training accuracy of 90.53% and a test accuracy of 90.88%, with an overfitting gap of only −0.35%. Furthermore, its cross-validation mean accuracy was 88.59% with a standard deviation of 0.69%, indicating superior generalization ability. As a result, CatBoost was selected as the first stage of the hybrid model,

https://doi.org/10.1021/acsaelm.5c00822
ACS Appl. Electron. Mater. 2025, 7, 6980−6993

ensuring minimal false classifications before proceeding to the regression phase.

3.6.2. Comparative Analysis and Performance Assessment of Regression Models. The second stage of the hybrid machine learning framework involved regression modeling to accurately quantify vitamin C concentrations based on electrochemical sensor responses. Following classification, where samples were identified as containing vitamin C, regression models were applied to predict the exact concentration levels. This phase was crucial for ensuring precise and reliable measurements, particularly in overcoming the inherent nonlinearity and variability in electrochemical signals.

To identify the most effective regression model, five widely used algorithms -XGBoost, LightGBM, CatBoost, RandomForest, and SVR- were evaluated using multiple performance metrics. The primary objective was to assess each model's predictive accuracy, robustness across different concentration levels, and generalization capability. The models were systematically compared using MAE that measures average prediction error; Root Mean Squared Error (RMSE) that penalizes larger deviations in prediction, R^2 Score that indicates how well the model explains variance in the data, Explained Variance Score that reflects the proportion of variance captured by the model and Cross-Validation R^2 Score that Ensures model generalizability across different subsets of data. The results obtained for each model are summarized in Figure 14.

The Hybrid Score was computed by integrating the performance metrics of the CatBoost classifier and regression models by eq 2. By combining the classification and regression metrics, the Hybrid Score provides a comprehensive evaluation of the hybrid model's overall effectiveness.

$$Hybrid\ Score = \frac{Regression\ R^2 + Classification\ F{-}1\ score}{2} \quad (2)$$

This approach ensures that the selected model not only accurately classifies the presence of vitamin C but also delivers highly reliable concentration predictions across varying analyte levels. The Hybrid Score thus serves as a holistic performance indicator, capturing both detection accuracy and quantitative precision within a unified metric. CatBoost demonstrated the highest predictive accuracy, with an R^2 Score of 0.5784 and the highest Hybrid Score (0.7609). It also exhibited the best generalization capability, as indicated by its Cross-Validation R^2 Score (0.5337). Conversely, SVR performed the weakest among all models, with significantly higher MAE (0.1070) and RMSE (0.1322), along with the lowest R^2 Score (0.0476). These results suggest that tree-based ensemble methods outperform traditional kernel-based regression models in handling the nonlinear characteristics of electrochemical sensor data.

To ensure optimal concentration prediction, the best-performing regression model was selected based on a combination of minimization of prediction errors (MAE and RMSE), maximization of R^2 Score and explained variance, generalization ability assessed via Cross-Validation R^2 Score and overall ranking using the Hybrid Score. Considering all these factors, CatBoost Regressor was chosen as the final regression model to be integrated into the hybrid framework. While LightGBM and XGBoost also demonstrated strong performance, CatBoost consistently achieved the most balanced trade-off between accuracy and model stability across different concentration ranges.

3.6.3. Integrated Performance Evaluation of the Hybrid Machine Learning Model. The CatBoost Classifier was selected as the best-performing classification model after an extensive comparison of multiple algorithms. The model was optimized using hyperparameters that were fine-tuned to enhance accuracy, recall, and overall predictive power. The final optimized parameters for classification were determined as iterations = 100, depth = 8, learning Rate = 0.1, L2 Leaf Regularization = 5, border count = 100 and class weights = {0:1.5, 1:0.5} for higher weight for class 0 to address class imbalance. The performance of the classification model was assessed using key evaluation metrics on both training and test data sets as given in Table 4.

Table 4. Performance Metrics for Hybrid Model's Classification

Metric	Train	Test
Accuracy	0.9413	0.8619
Precision	0.9529	0.9242
Recall	0.9820	0.9242
F1 Score	0.9672	0.9242

The classification accuracy of 86.19% on the test set confirms the model's strong generalization capability. The high recall score (0.9242 on the test set) ensures that vitamin C-positive samples are correctly detected, minimizing false negatives, while the precision score (0.9242) reduces false positives.

Following classification, the regression phase aimed to precisely estimate vitamin C concentration for positive samples ($C > 0$). The CatBoost Regressor emerged as the most effective model after hyperparameter optimization. The optimized parameters for regression were determined as iterations = 500, depth = 10, learning rate = 0.05, L2 Leaf Regularization = 3. The model's performance was evaluated based on multiple error minimization and predictive accuracy metrics as given in Table 5.

Table 5. Performance Metrics for Hybrid Model's Regression

Metric	CatBoost Regressor
MAE	0.0514
RMSE	0.0737
R^2 Score	0.7039
Explained Variance Score	0.7040
Cross-Validation R^2 Score	0.6396

The low MAE (0.0514) and RMSE (0.0737) values indicate that the model's predictions closely align with actual vitamin C concentrations, reducing absolute and squared errors. The R^2 Score (0.7039) and Explained Variance Score (0.7040) confirm that the regression model effectively captures nonlinear electrochemical sensor responses. The Cross-Validation R^2 Score (0.6396) ensures that the model generalizes well across different data partitions, enhancing stability in real-world applications.

The resulting Hybrid Score was 0.8141, indicating that the model maintained a strong balance between classification accuracy and regression precision. This metric ensured that

https://doi.org/10.1021/acsaelm.5c00822
ACS Appl. Electron. Mater. 2025, 7, 6980−6993

model selection prioritized both detection reliability and concentration estimation accuracy, making the hybrid system highly suitable for real-time electrochemical sensing applications.

4. CONCLUSIONS

This study presents the design, fabrication, and evaluation of an electrochemical sensor platform, integrating His-functionalized poly(2-hydroxyethyl methacrylate-*co*-ethylene glycol dimethacrylate) (His-pHEG) polymeric nanoparticles with Nafion-modified SPCE, for the sensitive and selective quantification of vitamin C. The synthesis of the His-pHEG nanoparticles, confirmed via comprehensive physicochemical characterization including FTIR, SEM, and zeta potential analyses, enabled the creation of a bioactive surface exhibiting enhanced affinity and selectivity toward vitamin C molecules. The incorporation of L-histidine onto the polymer backbone introduced functional imidazole groups, which facilitated specific interactions with vitamin C, contributing to the high analyte selectivity of the sensor system. Optimization of critical parameters, such as polymer concentration and Nafion film thickness, was systematically conducted to maximize the electrochemical response, as evidenced by CV and DPV measurements.

Under optimized conditions, the sensor demonstrated an impressive analytical performance, achieving a limit of detection (LoD) of 0.09 μM and a linear dynamic range between 0.28 and 11.36 μM, with a high correlation coefficient (R^2 = 0.9962). Validation experiments conducted using real lemon juice samples confirmed the sensor's practical applicability, with recovery rates consistently ranging from 98.1% to 103.1%. Furthermore, selectivity studies indicated that the developed His-pHEG/Nafion-modified SPCE sensor exhibited minimal cross-reactivity toward potentially interfering species, underscoring its high specificity for vitamin C detection in complex sample matrices.

In comparison with state-of-the-art systems reported in the literature (Table 1), the developed sensor demonstrated a lower detection limit and a comparable or broader linear range than previously reported platforms. Although many of these systems are not yet commercially available, they serve as current performance benchmarks. These results highlight the sensor's potential as a cost-effective, portable, and high-performance alternative suitable for real-world applications.

A distinguishing feature of this work is the incorporation of a novel hybrid ML framework to enhance the quantitative capabilities of the sensor. The two-stage ML approach—employing CatBoost-based classification for analyte detection and CatBoost Regressor for concentration estimation—successfully addressed the inherent nonlinearity and variability challenges associated with electrochemical measurements. The implementation of a Hybrid Score metric further facilitated a comprehensive, multidimensional evaluation of model performance, ensuring optimal model selection through a rigorous assessment of classification accuracy, regression precision, and stability.

Beyond its technical advancements, this study exemplifies a multidisciplinary approach, bridging the fields of polymer chemistry, electrochemical sensor engineering, and artificial intelligence-driven data analytics. The seamless integration of materials science and machine learning methodologies not only enhances analytical accuracy but also demonstrates a scalable and adaptable strategy applicable to diverse sensing contexts.

Looking forward, future research will focus on extending the applicability and portability of the developed system. Specifically, efforts will be directed toward integrating the sensor platform with mobile-based analytical devices, coupled with embedded ML algorithms, to facilitate real-time, on-site vitamin C detection in resource-limited settings. Furthermore, the modular design of both the polymeric nanostructure and computational framework offers significant potential for adaptation toward the detection of other clinically and industrially relevant analytes, thus broadening the scope and impact of the platform across various sectors including food safety, healthcare diagnostics, and pharmaceutical quality control.

AUTHOR INFORMATION

Corresponding Author

Emre Dokuzparmak − *Ege University, Faculty of Engineering, Bioengineering Department, Bornova 35040 İzmir, Türkiye;* orcid.org/0000-0002-0880-0235; Email: emre.dokuzparmak@ege.edu.tr

Authors

Emine Sezer − *Ege University, Faculty of Computer and Information Science, Computer Engineering Department, Bornova 35040 İzmir, Türkiye;* orcid.org/0000-0003-4776-6436

Timuçin Güner − *Ege University, Faculty of Science, Biochemistry Department, Bornova 35040 İzmir, Türkiye;* orcid.org/0000-0002-1033-1925

Esra Yaşar − *Ege University, Faculty of Science, Biochemistry Department, Bornova 35040 İzmir, Türkiye;* orcid.org/0009-0007-1011-8992

Hilal Özçelik − *Ege University, Faculty of Science, Biochemistry Department, Bornova 35040 İzmir, Türkiye;* orcid.org/0009-0007-8040-4038

Sinan Akgöl − *Ege University, Faculty of Science, Biochemistry Department, Bornova 35040 İzmir, Türkiye; Sabanci University, Nanotechnology Res. & Appl. Centre, Tuzla 34956 İstanbul, Türkiye*

Complete contact information is available at: https://pubs.acs.org/10.1021/acsaelm.5c00822

Notes

The authors declare no competing financial interest.

REFERENCES

(1) Van Hieu, T.; Guntoro, B.; Qui, N. H.; Quyen, N. T. K.; Al Hafiz, F. A. The application of ascorbic acid as a therapeutic feed additive to boost immunity and antioxidant activity of poultry in heat stress environment. *Vet. World* **2022**, *15*, 685.

(2) Varvara, M.; Bozzo, G.; Celano, G.; Disanto, C.; Pagliarone, C. N.; Celano, G. V. The use of ascorbic acid as a food additive: technical-legal issues. *Ital. J. Food Saf.* **2016**, *5*, DOI: 10.4081/ijfs.2016.4313.

(3) Njus, D.; Kelley, P. M.; Tu, Y. J.; Schlegel, H. B. Ascorbic acid: The chemistry underlying its antioxidant properties. *Free Radic. Biol. Med.* **2020**, *159*, 37−43.

(4) Santos, K. L.; Bragança, V. A.; Pacheco, L. V.; Ota, S. S.; Aguiar, C. P.; Borges, R. S. Essential features for antioxidant capacity of ascorbic acid (vitamin C). *J. Mol. Model.* **2022**, *28*, 1.

(5) Yin, X.; Chen, K.; Cheng, H.; Chen, X.; Feng, S.; Song, Y.; Liang, L. Chemical stability of ascorbic acid integrated into commercial

products: A review on bioactivity and delivery technology. *Antioxidants* **2022**, *11*, 153.
(6) Boo, Y. C. Ascorbic acid (vitamin C) as a cosmeceutical to increase dermal collagen for skin antiaging purposes: emerging combination therapies. *Antioxidants* **2022**, *11*, 1663.
(7) Jamshidovich, A. S. Ascorbic acid: its role in immune system, chronic inflammation diseases and on the antioxidant effects. *Eur. J. Mod. Med. Pract.* **2023**, *3*, 57−60.
(8) Jacques, H.; Jérôme, V.; Antoine, C.; Lucile, S.; Valérie, D.; Amandine, L.; Olivier, B. Prospective randomized study of the vitamin C effect on pain and complex pain regional syndrome after total knee arthroplasty. *Int. Orthop.* **2021**, *45*, 1155−1162.
(9) Bogdan, M.; Meca, A. D.; Boldeanu, M. V.; Gheorghe, D. N.; Turcu-Stiolica, A.; Subtirelu, M. S.; Surlin, P. Possible involvement of vitamin C in periodontal disease-diabetes mellitus association. *Nutrients* **2020**, *12*, 553.
(10) Zakić, T.; Budnar, M.; Kalezic, A.; Korać, A.; Janković, A.; Korać, B. Vitamin C biochemistry: From scurvy to COVID-19 treatment. *Hrana Ishrana* **2020**, *61*, 59.
(11) Kontoghiorghes, G. J.; Kolnagou, A.; Kontoghiorghe, C. N.; Mourouzidis, L.; Timoshnikov, V. A.; Polyakov, N. E. Trying to solve the puzzle of the interaction of ascorbic acid and iron: Redox, chelation and therapeutic implications. *Medicines* **2020**, *7*, 45.
(12) Carabotti, M.; Annibale, B.; Lahner, E. Common pitfalls in the management of patients with micronutrient deficiency: keep in mind the stomach. *Nutrients* **2021**, *13*, 208.
(13) Xu, D.; Chen, C.; Zhou, F.; Liu, C.; Tian, M.; Zeng, X.; Jiang, A. Vacuum packaging and ascorbic acid synergistically maintain the quality and flavor of fresh-cut potatoes. *LWT* **2022**, *162*, No. 113356.
(14) Rodríguez, G. M.; Sibaja, J. C.; Espitia, P. J.; Otoni, C. G. Antioxidant active packaging based on papaya edible films incorporated with Moringa oleifera and ascorbic acid for food preservation. *Food Hydrocoll.* **2020**, *103*, No. 105630.
(15) Otten, A. T.; Bourgonje, A. R.; Peters, V.; Alizadeh, B. Z.; Dijkstra, G.; Harmsen, H. J. Vitamin C supplementation in healthy individuals leads to shifts of bacterial populations in the gut—a pilot study. *Antioxidants* **2021**, *10*, 1278.
(16) Sadeghi, K.; Jee, H. W.; Paeng, K. J.; Seo, J. Photografting of conducting polymer onto polymeric substrate as non-migratory antioxidant packaging. *React. Funct. Polym.* **2021**, *158*, No. 104792.
(17) Bassi, M.; Lubes, G.; Bianchi, F.; Agnolet, S.; Ciesa, F.; Brunner, K. Ascorbic acid content in apple pulp, peel, and monovarietal cloudy juices of 64 different cultivars. *Int. J. Food Prop.* **2017**, *20* (Suppl.3), S2626−S2634.
(18) Manikandan, V. S.; Adhikari, B.; Chen, A. Nanomaterial based electrochemical sensors for the safety and quality control of food and beverages. *Analyst* **2018**, *143*, 4537−4554.
(19) Hall, M. G.; Lazard, A. J.; Grummon, A. H.; Mendel, J. R.; Taillie, L. S. The impact of front-of-package claims, fruit images, and health warnings on consumers' perceptions of sugar-sweetened fruit drinks: Three randomized experiments. *Prev. Med.* **2020**, *132*, No. 105998.
(20) Porto, I. S.; Neto, J. H. S.; dos Santos, L. O.; Gomes, A. A.; Ferreira, S. L. Determination of ascorbic acid in natural fruit juices using digital image colorimetry. *Microchem. J.* **2019**, *149*, No. 104031.
(21) Qiao, W.; Liu, Y.; Fan, X.; Yang, Y.; Liu, W.; Wang, L.; Li, L. Rapid and sensitive determination of ascorbic acid based on label-free silver triangular nanoplates. *Curr. Res. Food Sci.* **2023**, *7*, No. 100548.
(22) Nerdy, N. Determination of vitamin C in various colours of bell pepper (Capsicum annuum L.) by titration method. *Alchemy J. Penelit. Kim.* **2018**, *14*, 164−177.
(23) Yu, M.; Wen, R.; Jiang, L.; Huang, S.; Fang, Z.; Chen, B.; Wang, L. Rapid analysis of benzoic acid and vitamin C in beverages by paper spray mass spectrometry. *Food Chem.* **2018**, *268*, 411−415.
(24) Tulli, F.; Lemos, M. L.; Gutiérrez, D. R.; Rodríguez, S. D. C.; López de Mishima, B. A.; Paz Zanini, V. I. Electrochemical and spectrophotometric methods for polyphenol and ascorbic acid determination in fruit and vegetable extracts. *Food Technol. Biotechnol.* **2020**, *58*, 183−191.
(25) Škugor Rončević, I.; Skroza, D.; Vrca, I.; Kondža, A. M.; Vladislavić, N. Development and optimization of electrochemical method for determination of vitamin C. *Chemosensors* **2022**, *10*, 283.
(26) Jadav, J. K.; Umrania, V. V.; Rathod, K. J.; Golakiya, B. A. Development of silver/carbon screen-printed electrode for rapid determination of vitamin C from fruit juices. *LWT* **2018**, *88*, 152−158.
(27) Najwa, F. R.; Azrina, A. Comparison of vitamin C content in citrus fruits by titration and high performance liquid chromatography (HPLC) methods. *Int. Food Res. J.* **2017**, *24*, 726.
(28) Yu, M.; Wen, R.; Jiang, L.; Huang, S.; Fang, Z.; Chen, B.; Wang, L. Rapid analysis of benzoic acid and vitamin C in beverages by paper spray mass spectrometry. *Food Chem.* **2018**, *268*, 411−415.
(29) Spínola, V.; Llorent-Martínez, E. J.; Castilho, P. C. Determination of vitamin C in foods: Current state of method validation. *J. Chromatogr. A* **2014**, *1369*, 2−17.
(30) Mahato, K.; Wang, J. Electrochemical sensors: From the bench to the skin. *Sens. Actuators B Chem.* **2021**, *344*, No. 130178.
(31) Pani, D.; Achilli, A.; Spanu, A.; Bonfiglio, A.; Gazzoni, M.; Botter, A. Validation of polymer-based screen-printed textile electrodes for surface EMG detection. *IEEE Trans. Neural Syst. Rehabil. Eng.* **2019**, *27*, 1370−1377.
(32) Obaje, E. A.; Cummins, G.; Schulze, H.; Mahmood, S.; Desmulliez, M. P. Y.; Bachmann, T. T. Carbon screen-printed electrodes on ceramic substrates for label-free molecular detection of antibiotic resistance. *J. Interdiscip. Nanomed.* **2016**, *1*, 93−109.
(33) Bakker, E.; Telting-Diaz, M. Electrochemical sensors. *Anal. Chem.* **2002**, *74*, 2781−2800.
(34) Shoaib, A.; Darraj, A.; Khan, M. E.; Azmi, L.; Alalwan, A.; Alamri, O.; Khan, A. U. A nanotechnology-based approach to biosensor application in current diabetes management practices. *Nanomaterials* **2023**, *13*, 867.
(35) Suresh, R. R.; Lakshmanakumar, M.; Arockia Jayalatha, J. B. B.; et al. Fabrication of screen-printed electrodes: opportunities and challenges. *J. Mater. Sci.* **2021**, *56*, 8951−9006.
(36) Kamalasekaran, K.; Sundramoorthy, A. K. Applications of chemically modified screen-printed electrodes in food analysis and quality monitoring: a review. *RSC Adv.* **2024**, *14*, 27957−27971.
(37) Jaiswal, N.; Tiwari, I. Recent build outs in electroanalytical biosensors based on carbon-nanomaterial modified screen printed electrode platforms. *Anal. Methods* **2017**, *9*, 3895−3907.
(38) Jasmin, J. P.; Ouhenia-Ouadahi, K.; Miserque, F.; Dumas, E.; Cannizzo, C.; Chaussé, A. Straightforward grafting approach for cyclam-functionalized screen-printed electrodes for selective Cu (II) determination. *Electrochim. Acta* **2016**, *200*, 115−122.
(39) Mincu, N. B.; Lazar, V.; Stan, D.; Mihailescu, C. M.; Iosub, R.; Mateescu, A. L. Screen-printed electrodes (SPE) for in vitro diagnostic purpose. *Diagnostics* **2020**, *10*, 517.
(40) Dhara, K.; Debiprosad, R. M. Review on nanomaterials based screen printed electrodes in biosensing application. *J. Mater. Sci. Mater. Electron.* **2020**, *31*, 20718−20734.
(41) Rončević, I. Š.; Skroza, D.; Vrca, I.; Kondža, A. M.; Vladislavić, N. Development and optimization of electrochemical method for determination of vitamin C. *Chemosensors* **2022**, *10*, 283.
(42) Saylan, Y.; Akgönüllü, S.; Yavuz, H.; Ünal, S.; Denizli, A. Molecularly imprinted polymer based sensors for medical applications. *Sensors* **2019**, *19*, 1279.
(43) Liu, X.; Ren, J.; Su, L.; Gao, X.; Tang, Y.; Ma, T.; Li, J. Novel hybrid probe based on double recognition of aptamer-molecularly imprinted polymer grafted on upconversion polymeric nanoparticles for enrofloxacin sensing. *Biosens. Bioelectron.* **2017**, *87*, 203−208.
(44) Zhang, Y.; Yu, B.; Ma, S.; Ma, Y.; Zhang, G.; Hu, K.; Zhou, F. Engineering Surface-Grafted Polymers for Adhesion and Friction Control. *Prog. Polym. Sci.* **2024**, *157*, 101888.
(45) Wang, S.; Wang, Z.; Li, J.; Li, L.; Hu, W. Surface-grafting polymers: from chemistry to organic electronics. *Mater. Chem. Front.* **2020**, *4*, 692−714.
(46) Zhou, X.; Essawy, H. A.; Mohamed, M. F.; Ibrahim, H. S.; Ammar, N. S. Grafting polymerization of acrylic acid onto chitosan-

https://doi.org/10.1021/acsaelm.5c00822
ACS Appl. Electron. Mater. 2025, 7, 6980−6993

cellulose hybrid and application of the graft as highly efficient ligand for elimination of water hardness: Adsorption isotherms, kinetic modeling and regeneration. *J. Environ. Chem. Eng.* **2018**, *6*, 2137−2147.
(47) Wang, Y.; Wu, C. Site-specific conjugation of polymers to proteins. *Biomacromolecules* **2018**, *19*, 1804−1825.
(48) Zhang, Z.; Shan, R.; Muhammad, W. T.; Zhang, H. Recent advances in recognition molecule-based detection methods for prevention and monitoring of estrogen disruptors related food fraud. *Trends Food Sci. Technol.* **2024**, *146*, 104395.
(49) Apostolopoulos, I.; Androulakis, S.; Kalkavouras, P.; Fouskas, G.; Pandis, S. Calibration and inter-unit consistency assessment of an electrochemical sensor system using machine learning. *Sensors* **2024**, *24*, 4110.
(50) Zuidema, C.; Schumacher, C.; Austin, E.; Carvlin, G.; Larson, T.; Spalt, E.; Sheppard, L. Deployment, calibration, and cross-validation of low-cost electrochemical sensors for carbon monoxide, nitrogen oxides, and ozone for an epidemiological study. *Sensors* **2021**, *21*, 4214.
(51) Lavrentev, F.; Rumyantsev, I.; Ivanov, A.; Shilovskikh, V.; Orlova, O.; Nikolaev, K.; Skorb, E. Soft hydrogel actuator for fast machine-learning-assisted bacteria detection. *ACS Appl. Mater. Interfaces* **2022**, *14*, 7321−7328.
(52) Zhu, S.; Sun, X.; Gao, X.; Wang, J.; Zhao, N.; Sha, J. Equivalent circuit model recognition of electrochemical impedance spectroscopy via machine learning. *J. Electroanal. Chem.* **2019**, *855*, No. 113627.
(53) Hoar, B. B.; Zhang, W.; Chen, Y.; Sun, J.; Sheng, H.; Zhang, Y.; Liu, C. Redox-detecting deep learning for mechanism discernment in cyclic voltammograms of multiple redox events. *ACS Electrochem.* **2025**, *1*, 52−62.
(54) Boateng, E.; Otoo, J.; Abaye, D. Basic tenets of classification algorithms k-nearest-neighbor, support vector machine, random forest and neural network: a review. *J. Data Anal. Inf. Process.* **2020**, *8*, 341−357.
(55) Ren, Z.; Yang, K.; Dong, W. Spatial analysis and risk assessment model research of arthritis based on risk factors: China, 2011, 2013 and 2015. *IEEE Access* **2020**, *8*, 206406−206417.
(56) Yap, S.; Pan, J.; Dao, V.; Zhang, X.; Wang, X.; Teo, W.; Thean, A. Engineered nucleotide chemicapacitive microsensor array augmented with physics-guided machine learning for high-throughput screening of cannabidiol. *Small* **2022**, *18*, 2107659.
(57) Wang, Z.; Dong, W.; Yang, K. Spatiotemporal analysis and risk assessment model research of diabetes among people over 45 years old in China. *Int. J. Environ. Res. Public Health* **2022**, *19*, 9861.
(58) Kang, M.; Kim, D.; Kim, J.; Kim, N.; Lee, S. Strategies to Enrich Electrochemical Sensing Data with Analytical Relevance for Machine Learning Applications: A Focused Review. *Sensors* **2024**, *24*, 3855.
(59) Tuniya, N.; Parihar, M.; Patil, S.; Lawand, K. Comparative Analysis of Regressor. *Proceedings of International Conference on Computing and Communication Networks*: ICCCN 2021; Springer Nature, 2022; Vol. *394*, p 209.
(60) Qin, A.; Fan, Z.; Zhang, L. Information entropy-based hybrid models improve the accuracy of reference evapotranspiration forecast. *Adv. Meteorol.* **2024**, *2024*, 1−13.
(61) Guo, F.; Mo, H.; Wu, J.; Pan, L.; Zhou, H.; Zhang, Z.; Huang, F. A hybrid stacking model for enhanced short-term load forecasting. *Electronics* **2024**, *13*, 2719.
(62) Kang, J.; Choi, Y.; Kim, I.; Lee, H.; Kim, H.; Baik, S.; Lee, K. Lasso-based machine learning algorithm for prediction of lymph node metastasis in T1 colorectal cancer. *Cancer Res. Treat.* **2021**, *53*, 773−783.
(63) Shrivastava, A.; Gupta, V. B. Methods for the determination of limit of detection and limit of quantitation of the analytical methods. *Chron. Young Sci.* **2011**, *2*, 21−25.
(64) Dennany, L.; Gerlach, M.; O'Carroll, S.; Keyes, T. E.; Forster, R. J.; Bertoncello, P. Electrochemiluminescence (ECL) sensing properties of water soluble core-shell CdSe/ZnS quantum dots/Nafion composite films. *J. Mater. Chem.* **2011**, *21*, 13984−13990.
(65) Wang, Q.; Xiao, X.; Hu, X.; Huang, L.; Li, T.; Yang, M. Molecularly imprinted electrochemical sensor for ascorbic acid determination based on MXene modified electrode. *Mater. Lett.* **2021**, *285*, No. 129158.
(66) Sanker, S. S.; Thomas, S.; Jacob, D. P.; Suniya, V. S.; Nalini, S.; Madhusoodanan, K. N. Highly sensitive colorimetric detection of ascorbic acid using molecularly imprinted photonic crystal hydrogel sensor. *Microchem. J.* **2024**, *206*, No. 111435.
(67) Zhao, X.; Zhang, W.; Chen, H.; Chen, Y.; Huang, G. Disposable electrochemical ascorbic acid sensor based on molecularly imprinted poly (o-phenylenediamine)-modified dual channel screen-printed electrode for orange juice analysis. *Food Anal. Methods* **2014**, *7*, 1557−1563.
(68) Cao, F.; Zhang, L.; Tian, Y. A novel N-doped carbon nanotube fiber for selective and reliable electrochemical determination of ascorbic acid in rat brain microdialysates. *J. Electroanal. Chem.* **2016**, *781*, 278−283.
(69) Mangiacotte, N.; Prosperi-Porta, G.; Liu, L.; Dodd, M.; Sheardown, H. Mucoadhesive nanoparticles for drug delivery to the anterior eye. *Nanomaterials* **2020**, *10*, 1400.
(70) Zagni, C.; Coco, A.; Dattilo, S.; Patamia, V.; Floresta, G.; Fiorenza, R.; Rescifina, A. HEMA-based macro and microporous materials for CO2 capture. *Mater. Today Chem.* **2023**, *33*, No. 101715.
(71) Ghosh, A.; Tucker, M. J.; Gai, F. 2D IR spectroscopy of histidine: probing side-chain structure and dynamics via backbone amide vibrations. *J. Phys. Chem. B* **2014**, *118*, 7799−7805.
(72) Fu, D.; Dong, Y.; Yin, J.; Zhang, B.; Zhang, S.; Deng, J.; Liu, X. A Multi-Channel Handheld Diagnostic Device Based on Green Biomimetic Material for Point-of-Care Testing of Vitamin C in Human Fluids. *Adv. Healthcare Mater.* **2025**, *14* (3), No. 2403454.
(73) Gao, X.; Chen, S.; Wang, X.; Liu, H.; Wang, X. A Portable Nanoporous Gold Modified Screen-Printed Sensor for Reliable and Simultaneous Multi-Vitamins Analysis. *Chemosensors* **2023**, *11* (9), 502.
(74) Bettazzi, F.; Ingrosso, C.; Sfragano, P. S.; Pifferi, V.; Falciola, L.; Curri, M. L.; Palchetti, I. Gold nanoparticles modified graphene platforms for highly sensitive electrochemical detection of vitamin C in infant food and formulae. *Food Chem.* **2021**, *344*, No. 128692.
(75) Sezer, E.; Dokuzparmak, E.; Özçelik, H.; Yaşar, E.; Kaya, T.; Güner, T.; Akgöl, S. Harnessing Machine Learning to Revolutionize Electrochemical Detection of Vitamin E Acetate in E-Liquids. *ACS Omega.* **2025**, *10*, 27098.

https://doi.org/10.1021/acsaelm.5c00822
ACS Appl. Electron. Mater. 2025, 7, 6980−6993